Title
Long-term thermal effects on injectivity evolution during CO2 storage

Authors
Vilarrasa, Victor
Rinaldi, Antonio P
Rutqvist, Jonny

Publication Date
2017-09-01

DOI
10.1016/j.ijggc.2017.07.019

Peer reviewed

LONG-TERM THERMAL EFFECTS ON INJECTIVITY EVOLUTION DURING CO_2 STORAGE

Victor Vilarrasa[a,b,c,*], Antonio P. Rinaldi[a,d] and Jonny Rutqvist[a]

(a) Earth and Environmental Sciences Area, Lawrence Berkeley National Laboratory, CA, USA

(b) Institute of Environmental Assessment and Water Research, Spanish National Research Council (IDAEA-CSIC), Barcelona, Spain

(c) Associated Unit: Hydrogeology Group (UPC-CSIC), Barcelona, Spain

(d) Swiss Seismological Service, Swiss Federal Institute of Technology, ETHZ, Zürich, Switzerland

Accepted for Publication July 21, 2017

International Journal of Greenhouse Gas Control

https://doi.org/10.1016/j.ijggc.2017.07.019

(*) Corresponding author at: victor.vilarrasa@idaea.csic.es

ABSTRACT

Carbon dioxide (CO_2) is likely to reach the bottom of injection wells at a colder temperature than that of the storage formation, causing cooling of the rock. This cooling, together with overpressure, tends to open up fractures, which may enhance injectivity. We investigate cooling effects on injectivity enhancement by modeling the In Salah CO_2 storage site and a theoretical, long-term injection case. We use stress-dependent permeability functions that predict an increase in permeability as the effective stress acting normal to fractures decreases. Normal effective stress can decrease either due to overpressure or cooling. We calibrate our In Salah model, which includes a fracture zone perpendicular to the well, obtaining a good fitting with the injection pressure measured at KB-502 and the rapid CO_2 breakthrough that occurred at the observation well KB-5 located 2 km away from the injection well. CO_2 preferentially advances through the fracture zone, which becomes two orders of magnitude more permeable than the rest of the reservoir. Nevertheless, the effect of cooling on the long-term injectivity enhancement is limited in pressure dominated storage sites, like at In Salah, because most of the permeability enhancement is due to overpressure. However, thermal effects enhance injectivity in cooling dominated storage sites, which may decrease the injection pressure by 20 %, saving a significant amount of compression energy all over the duration of storage projects. Overall, our simulation results show that cooling has the potential to enhance injectivity in fractured reservoirs.

Keywords: cooling; fracture aperture; permeability increase; thermo-hydro-mechanical coupling

INTRODUCTION

Carbon dioxide (CO_2) is likely to reach the bottom of the injection well at a colder temperature than that of the storage formation. This temperature difference occurs because CO_2 does not

2

thermally equilibrate with the geothermal gradient, especially at high flow rates of injection (Paterson et al., 2008). For example, the temperature difference between the temperature at which CO_2 entered the storage formation and the rock was of 55 ºC at Cranfield, Mississippi (Kim and Hosseini, 2014) and of 45 ºC at In Salah, Algeria (Bissell et al., 2011). Despite these large temperature differences, thermal effects have received little attention and only a few studies deal with them (Han et al., 2010; Singh et al., 2011; Goodarzi et al., 2012, 2015; Fang et al., 2013; Bao et al., 2014; Vilarrasa, 2016; Vilarrasa and Rutqvist, 2017). In particular, the geomechanical effects of cold CO_2 injection on caprock stability have been investigated in a generic repository (Vilarrasa et al., 2013a; 2014; Kim and Hosseini, 2015) and at the In Salah storage site (Preisig and Prevost, 2011; Gor et al., 2013; Vilarrasa et al., 2015).

Apart from the significant temperature difference, a substantial overpressure (around 10 MPa) caused relevant thermo-hydro-mechanical coupled effects at the In Salah storage site (Gemmer et al., 2012; Verdon et al., 2013; White et al., 2014; Rutqvist et al., 2016). A ground uplift of around 5 mm/yr was measured on top of the three horizontal injection wells using satellite geodetic data (Vasco et al., 2008; Mathieson et al., 2009; Onuma and Okhawa, 2009). Simulation results showed that such ground uplift rate could be reproduced by considering pressure increase and volumetric expansion of both the injection zone and the overlying caprock (Rutqvist et al., 2010). This uplift rate would require the caprock permeability to be two orders of magnitude higher than the initially estimated value from core samples (Rutqvist et al., 2010). Furthermore, a double lobe uplift pattern appeared on top of KB-502 injection well, which was explained by the opening of a fracture zone at depth (Vasco et al., 2010). The opening of this fracture zone might have induced some microseismic events (Oye et al., 2013), but no felt seismic event has been reported (IEAGHG, 2013; Stork et al., 2015; Verdon et al., 2015). A number of detailed analyses and modeling of this fracture zone opening and resulting surface uplift pattern have indicated

3

that the fracture zone opening remained confined within the lowest few hundred meters of the 900 m thick caprock, so the overall sealing capacity of the caprock was not compromised (Vasco et al., 2010; Rinaldi and Rutqvist, 2013).

An event that deserves special attention is the CO_2 leakage that occurred through an existing well (KB-5), located 2 km away from the KB-502 injection well. After the leakage at KB-5 was detected around 2 years after injection started, the well was properly sealed to avoid further leakage (Ringrose et al., 2009). This rapid breakthrough probably occurred because of reservoir permeability enhancement caused by fracture opening as a result of overpressure and cooling induced by injection (Birkholzer et al., 2015). In a fractured reservoir, like that at In Salah, both overpressure, which expands fractures, and cooling, which contracts the matrix, open up fractures (de Simone et al., 2013) and thus, injectivity is expected to increase.

The aim of this study is to investigate the role of thermal contraction of the rock on permeability enhancement. To this end, we perform coupled thermo-hydro-mechanical simulations of cold CO_2 injection modeling the In Salah storage site. First, we analyze the cooling front advance in a fractured reservoir by modeling a single fracture surrounded by rock matrix. Next, we simulate injection at the In Salah storage site using an equivalent continuum model to account for fractures and considering reactivation and opening of the fracture zone, providing a preferential flow path for the injected CO_2. In particular, we calibrate our model to reproduce the injection pressure measured at KB-502 and the CO_2 breakthrough at the observation well KB-5. Finally, we study the role of induced thermal stresses on injectivity enhancement for both In Salah and a theoretical, long-term injection case.

 4

METHODS

Thermo-hydro-mechanical mathematical model

We consider both CO_2 injection in thermal equilibrium with the storage formation and injection of CO_2 that is colder than the storage formation. Injection of cold CO_2 in a deep confined saline formation induces coupled thermo-hydro-mechanical processes that may affect reservoir injectivity. Thus, mass conservation of each phase, energy balance and momentum balance have to be solved to account for these couplings. Mass conservation of these two partially miscible fluids can be written as (Bear, 1972)

$$\frac{\partial(\phi S_\alpha \rho_\alpha)}{\partial t} + \nabla \cdot (\rho_\alpha \mathbf{q}_\alpha) = r_\alpha, \qquad \alpha = c, w, \tag{1}$$

where ϕ [L^3 L^{-3}] is porosity, S_α [-] is saturation of the α-phase, ρ_α [M L^{-3}] is density of the α-phase, t [T] is time, $\mathbf{q}_\alpha$ [L^3 L^{-2} T^{-1}] is the volumetric flux, r_α [M L^{-3} T^{-1}] is the phase change term (i.e., CO_2 dissolution into water and water evaporation into CO_2) (Spycher and Pruess, 2005) and α is either CO_2-rich phase, c, or aqueous phase, w.

Momentum conservation for the CO_2-rich and the aqueous phases is given by Darcy's law

$$\mathbf{q}_\alpha = -\frac{\kappa \kappa_{r\alpha}}{\mu_\alpha}(\nabla P_\alpha + \rho_\alpha g \nabla z), \qquad \alpha = c, w, \tag{2}$$

where κ [L^2] is intrinsic permeability, $\kappa_{r\alpha}$ [-] is the α-phase relative permeability, μ_α [M L^{-1} T^{-1}] is viscosity of α-phase, P_α [M L^{-1} T^{-2}] is the α-phase pressure, g [L T^{-2}] is gravity and z [L] is the vertical coordinate.

Energy conservation can be written as (e.g., Nield and Bejan, 2006)

$$\frac{\partial((1-\phi)\rho_s h_s + \phi \rho_w S_w h_w + \phi \rho_c S_c h_c)}{\partial t} - \phi S_c \frac{DP_c}{Dt} + \nabla \cdot (-\lambda \nabla T + \rho_w h_w \mathbf{q}_w + \rho_c h_c \mathbf{q}_c) = 0, \tag{3}$$

5

where ρ_s [M L^{-3}] is solid density, h_α [L^2 T^{-2}] is enthalpy of α -phase ($\alpha = c, w, s$; s for solid), λ [M L T^{-3} Θ] is thermal conductivity of the geological media and T [Θ] is temperature. We assume thermal equilibrium of all phases at every point.

Neglecting inertial terms, the momentum balance of the solid phase is reduced to the equilibrium of stresses

$$\nabla \cdot \boldsymbol{\sigma} + \mathbf{b} = \mathbf{0}, \quad (4)$$

where $\boldsymbol{\sigma}$ [M L^{-1} T^{-2}] is the stress tensor and $\mathbf{b}$ [M L^{-2} T^{-2}] is the body forces vector.

We assume linear thermoelasticity in porous media to include the effect of changes in fluid pressure and temperature on rock strain. Elastic strain is a function of total stress, overpressure and temperature (Segall and Fitzgerald, 1998),

$$\boldsymbol{\varepsilon} = \frac{1}{2G}\boldsymbol{\sigma} - \left(\frac{1}{2G} - \frac{1}{3K}\right)\sigma_m \mathbf{I} - \frac{1}{3K}\Delta P \mathbf{I} - \alpha_T \Delta T \mathbf{I}, \quad (5)$$

where $\boldsymbol{\varepsilon}$ [L L^{-1}] is the strain tensor, $\sigma_m = tr(\boldsymbol{\sigma})/3$ [M L^{-1} T^{-2}] is the mean stress, $tr(\boldsymbol{\sigma})$ [M L^{-1} T^{-2}] is the trace of the stress tensor, $\mathbf{I}$ [-] is the identity matrix, P [M L^{-1} T^{-2}] is fluid pressure, $K = E/(3(1-2\nu))$ [M L^{-1} T^{-2}] is the bulk modulus, $G = E/(2(1+\nu))$ [M L^{-1} T^{-2}] is the shear modulus, E [M L^{-1} T^{-2}] is the Young's modulus, ν [-] is Poisson ratio and α_T [Θ^{-1}] is the linear thermal expansion coefficient of the porous medium. We adopt the sign criterion of geomechanics, i.e., stress and strain are positive in compression and negative in extension.

The volumetric strain, ε_v [L L^{-1}], reads

$$\varepsilon_v = \frac{\sigma_m'}{K} - 3\alpha_T \Delta T, \quad (6)$$

where σ_m' [M L^{-1} T^{-2}] is the mean effective stress. Combining Equations (5) and (6), the effective stress, $\boldsymbol{\sigma}'$ [M L^{-1} T^{-2}], changes yield

6

$$\boldsymbol{\sigma}' = K\varepsilon_v \mathbf{I} + 2G\left(\boldsymbol{\varepsilon} - \frac{\varepsilon_v}{3}\mathbf{I}\right) + 3K\alpha_T \Delta T \mathbf{I} \ . \qquad (7)$$

These effective stress changes induce changes in fracture aperture and consequently, in permeability and capillarity (Rutqvist et al., 2002; Rutqvist, 2015).

<u>Stress-dependent permeability</u>

We assume that fracture aperture depends on the normal effective stress acting on the fracture according to an exponential relation (Liu et al., 2013; Liu and Rutqvist, 2013). We adopt the conceptual model initially proposed by Liu et al. (2009), which divides fractured geological media into a soft and a hard part. The soft part represents the response of a medium to small stress, and it follows a “natural” or “true” strain formulation in Hooke’s law. The hard part represents the rock response to large stress, following a so-called “engineering” strain relationship for the Hooke’s law. Liu et al. (2013) verified this model by comparison to experimental data on fracture closure as a function of stress. Liu and Rutqvist (2013) extended such formulation to a dual continuum model (i.e., accounting for fractures and rock matrix, both represented with soft and hard part). Assuming that most deformation occurs at cracks or fractures and that it is poorly affected at large stress, together with the assumption that the cubic law holds valid (Witherspoon et al., 1980), permeability change can then be evaluated accounting for the initial state of stress as (Rinaldi et al., 2014a)

$$\frac{\kappa_{hm}}{\kappa_i} = \left(\frac{b}{b_i}\right)^3 = \left(\frac{\gamma_e + \gamma_t e^{\frac{\sigma'_n}{K_{t,f}}}}{\gamma_e + \gamma_t e^{\frac{\sigma'_{n,i}}{K_{t,f}}}}\right)^3 , \qquad (8)$$

where b [L] and b_i [L] are the current and initial fracture apertures, respectively, and κ_{hm} [L^2] and κ_i [L^2] are the permeability at the current and initial stress state, respectively. $K_{t,f}$

7

[M L^{-1} T^{-2}] refers to the bulk modulus of the reservoir fractures, and σ'_n [M L^{-1} T^{-2}] and $\sigma'_{n,i}$ [M L^{-1} T^{-2}] are the current and initial normal effective stress acting on the fracture, respectively (Rinaldi et al., 2014a). γ_e [L^3 L^{-3}] and γ_t [L^3 L^{-3}] represent the unstressed volume fraction for the hard and soft parts of a body rock, respectively (Liu and Rutqvist, 2013).

We further assume permeability changes due to fracture zone reactivation. In comparison to the fix permeability increase proposed by Rinaldi et al. (2016), here if fracture reactivation occurs, the permeability may follow a similar stress-dependent permeability curve as that of Equation (8), but with different $K_{t,f}$, γ_e, and γ_t (Figure 1). To calculate fracture reactivation, we consider the Mohr-Coulomb failure criterion, which in terms of the maximum, σ_1' [M L^{-1} T^{-2}], and minimum, σ_3' [M L^{-1} T^{-2}], principal effective stresses reads

$$f = \sigma_1' - \frac{1+\sin\varphi}{1-\sin\varphi}\sigma_3', \qquad (9)$$

where φ [-] is the friction angle. If reactivation occurs, i.e., $f = 0$, permeability is enhanced (Figure 1).

Modeling of In Salah, Algeria

Fracture model

We firstly model non-isothermal two-phase flow, with no mechanical coupling, in a single fracture (Figure 2) in order to analyze the effect of fractures on the fluid pressure and temperature distributions. Such model is needed to assess the validity (i.e., if the pressure and temperature distributions could be affected by preferential flow through fractures) of a porous media model that does not explicitly include fractures. Due to symmetry, the model includes half of the fracture and half of the rock matrix between two consecutive fractures. We consider two

8

models, one for the minimum spacing of 0.2 m (the model is 0.1 m wide) and another one for the maximum spacing of 1.0 m (the model is 0.5 m wide) of the fracture spacing at In Salah (Iding and Ringrose, 2010). We consider that the aperture of the fracture equals 10^{-3} m, which is within the range of fracture aperture at In Salah (Iding and Ringrose, 2010). The length of the model is 500 m. We impose a constant pressure and temperature at the boundaries coinciding with the injection well and at the outer boundary. While we prescribe the pressure at 30 MPa and the temperature at 50 ºC at the injection well, we maintain the initial conditions at the outer boundary, i.e., a pressure of 18 MPa and a temperature of 95 ºC. Table 1 includes the hydro-thermal properties of the fracture and the rock matrix. The capillary functions of the rock matrix fit the retention curve and relative permeability curves measurements performed on the reservoir rock of In Salah, which were presented by Shi et al. (2012).

<u>In Salah model</u>

Then, to investigate the effect of cold CO_2 injection on injectivity, we model the injection of CO_2 through well KB-502 at In Salah, Algeria. Since we aim to study how thermo-hydro-mechanical effects induce changes in injectivity, we focus on the storage formation. We model a 2D horizontal section of the storage formation under plane strain conditions, which is representative of the central section of the storage formation. The model extends 76x76 km^2, with open flow boundary conditions and no displacement perpendicular to the outer boundaries (Figure 3). The model includes a fracture zone that extends 3500 m in the direction perpendicular to the injection well and that has a width of 80 m (Figure 3) (Rinaldi and Rutqvist, 2013; Rucci et al., 2013). Injection induced pressure inflation and opening of this fracture zone caused the double lobe uplift observed on the surface at In Salah (Vasco et al., 2010) and is thought to have enabled the rapid CO_2 breakthrough observed at well KB-5 (Ringrose et al., 2009). The initial fluid pressure is 18.0 MPa, the temperature 95 ºC, the vertical stress is 40.5 MPa, the maximum horizontal

9

stress is 45.5 MPa (perpendicular to the horizontal injection well) and the minimum horizontal stress is 28.6 MPa (parallel to the well) (Morris et al., 2011). Injection takes places in a 1000 m injection well, which is centered in the model. The injection rate closely follows the actual injection rate of 0.3 Mt/yr at KB-502 (Rinaldi and Rutqvist, 2013). CO_2 is injected 45 ºC colder than the storage formation, which corresponds to the actual injection temperature at In Salah (Bissell et al., 2011).

The storage formation at In Salah is characterized by a set of fractures perpendicular to the minimum principal stress, i.e., perpendicular to the horizontal injection well (Iding and Ringrose, 2010). The fracture aperture has been estimated to range from 10^{-4} m to 10^{-3} m and the spacing from 0.2 m to 1.0 m (Iding and Ringrose, 2010). Our reservoir model includes these data in the calculation of the permeability (Equation (8)), but fractures are not explicitly included in the model.

We consider that the higher fracture density within the fracture zone yields a lower stiffness and a higher permeability. To determine the material properties of both the fracture zone and the rest of the reservoir, we calibrate the model to fit the temporal evolution of bottomhole pressure at KB-502 and the breakthrough of CO_2 after about 2 years from the beginning of injection at point P6. P6 is placed 2 km away from the well and around 100 m away from the center of the fracture zone (see Figure 3), which corresponds to the approximate position of well KB-5 at In Salah.

In Salah model calibration

Since no real measurements of the bottomhole pressure were carried out during active operation, we calculate the bottomhole pressure from the wellhead pressure and the injection rate measurements by using the code T2Well (Pan et al., 2011). Given the uncertainties in this calculation, we assume that an error of 2 MPa on the computed pressure may exist. The parameters that are calibrated are the (i) initial permeability, (ii) the parameter $K_{t,f}$, (iii) the

10

volume fractions γ_e and γ_t, and (iv) the friction angle for both the reservoir and fracture zone. The volume fraction of the hard part of the body rock γ_e is assumed to change from 0.001 to 0.2647 and the volume fraction of the soft part of the body rock γ_t from 0.7353 to 0.999, with the restriction that $\gamma_e + \gamma_t = 1$. For the calibration, real measurement of injection rates at In Salah were used as input for the model (Rinaldi et al., 2016)

The model is calibrated by matching the pressure at the KB-502 injection well and by obtaining CO_2 breakthrough at well KB-5 around 2 years after the start of injection. Data matching is performed with the code iTOUGH2-PEST with TOUGH-FLAC (Rinaldi et al., 2015a; 2016). This approach takes advantage of the iTOUGH2 capabilities (Finsterle, 2004) for inverse analysis of a forward model through the PEST protocol (Finsterle and Zhang, 2011). Coupled fluid flow and geomechanics simulations are carried out using TOUGH-FLAC (Rutqvist, 2011). TOUGH-FLAC combines the multiphase, multicomponent fluid flow and heat transport simulator TOUGH2 (Pruess et al., 2011) and the geomechanical simulator FLAC^{3D} (ITASCA, 2009). TOUGH2 uses in these simulations the equation of state ECO2N, which accounts for mixtures of water, NaCl and CO_2, as well as dissolution of CO_2 into water (Pruess, 2005). TOUGH-FLAC has been applied to several problems of CO_2 injection in deep saline formation implying deformation and two-phase flow under isothermal (e.g., Rinaldi et al., 2014b, 2015b) and non-isothermal conditions (Rutqvist et al., 2011).

<u>Modeling of thermal effects for In Salah reservoir</u>

Once the model is calibrated for the initial injection period, which lasted for around 2 years, at injection well KB-502 at In Salah, we perform generic simulations to study the hypothetical thermal effects that could have occurred for a long-term CO_2 injection at a constant mass flow rate of 0.3 Mt/yr maintained during 30 years. This injection rate is similar to the one injected at

11

In Salah and induces a fluid pressure that is very close to fracturing conditions through the entire injection period. We run a base case using the same properties as the calibrated model, injecting CO_2 at 50 °C. Then, to investigate the effect of thermo-mechanical induced stresses (the third term on the right-hand side of Equation (7)) on injectivity, we run a case in isothermal conditions. Furthermore, since induced thermal stresses are proportional to the stiffness of the rock, we run two additional simulations of CO_2 injection at 50 °C, in which the stiffness of the fracture zone is increased by a factor of 5 and 10.

Modeling of thermal effect for a generic, high permeable reservoir

Finally, we model a case with a homogeneous high reservoir permeability ($\kappa = 10^{-13}$ m^2 in the fracture zone and the rest of the reservoir) and with a Young’s modulus equal to 10 GPa in the whole model, so that pressure buildup is low and the changes in injectivity are induced mainly by cooling.

RESULTS

Fracture model

Figure 4 shows the temperature distribution with distance to the injection well after 3 days of CO_2 injection at 50 °C in a model that includes one fracture and 0.5 m of rock matrix. The temperature profile and temperature front shows a negligible difference between the fracture and the rock matrix. In spite of the fact that CO_2 advances slightly more rapidly through the fracture due to its higher permeability, the relatively high permeability of the rock matrix allows homogenizing the cooling front and there is no preferential advance through the fracture. This homogeneous front is observed for the models that consider a fracture spacing of 0.2 m and 1.0

12

m. For the model with smaller fracture spacing, i.e., 0.2 m, no temperature difference is observed in the direction perpendicular to the fracture. For the model with larger fracture spacing, i.e., 1.0 m, a slight difference of 0.01 °C is observed between the temperature at the fracture and the temperature at a midpoint between two fractures, i.e., 0.5 m away from the fracture inside the rock matrix. This verification validates the assumption of modeling the reservoir at In Salah, which is fractured with fractures perpendicular to the injection well, as an equivalent porous media in which fractures do not need to be explicitly included in the model.

In Salah reservoir model calibration

Figure 5 shows the simulated pressure resulting from the calibration of CO_2 injection at well KB-502 at In Salah. We achieved a reasonable fit during active injection phase, with a bottomhole pressure that follows the measured pressure evolution. Nevertheless, pressure drop is lower in our model than in the measurements after shut-in, which is likely due to the fact that our injection well model does not account for the vertical part of the well, so it does not simulate processes such as phase transition that may occur after shut-in. Thus, the error of the computed bottomhole pressure from the wellhead pressure measurements may entail a larger error after shut-in than during the injection phase, which could explain the mismatch. Table 2 lists the calibrated parameters and their values.

To reproduce not only the pressure evolution, but also the CO_2 breakthrough at well KB-5 (point P6 in our model), the resulting permeability within the fracture zone is much larger than in the rest of the reservoir. Figure 6 displays the stress-dependent permeability functions of both the fracture zone and the rest of the reservoir, including the permeability enhancement upon fracture reactivation. Fault or fracture zone reactivation may cause shear slip of numerous fractures, which open up due to shear dilatancy, and thereby enhance the overall fracture zone permeability (Yeo et al., 1998; Mallikamas and Rajaram, 2005; Vilarrasa et al., 2011; Rutqvist, 2015). The

13

permeability evolution at points P1 to P4 (see Figure 3 for the location of the points) is also plotted. Permeability increases as the effective stress normal to the fractures decreases as a result of overpressure and cooling. Permeability increases up to two orders of magnitude in the fracture zone, reaching values as high as 10^{-11} m^2. In contrast, the permeability in the rest of the reservoir increases up to $2 \cdot 10^{-14}$ m^2, i.e., just by a factor of three, which is in accordance with previous estimates of permeability increase at In Salah (Rinaldi and Rutqvist, 2013; Liu and Rutqvist, 2013).

This permeability contrast between the fracture zone and the rest of the reservoir causes a preferential advance of CO_2 through the fracture zone (Figure 7b). The CO_2 plume reaches point P3 (located 250 m away from the injection well inside the fracture zone) in 1 month and point P5 (located 2500 m away from the injection well inside the fracture zone) in around 1 year (Figure 5c). This rapid advance of the CO_2 plume within the fracture zone results in CO_2 breakthrough at well KB-5 2.3 years after the start of injection. The time of the breakthrough is within the temporal scale at which CO_2 breakthrough was observed in the field (Ringrose et al., 2009). In contrast, CO_2 advances much slower outside the fracture zone. Actually, CO_2 does not reach point P2, which is placed only 250 m away from the injection well outside the fracture zone.

Figure 5 shows that the cooling front advances much behind than the CO_2 front. Due to the limited advance of CO_2 outside of the fracture zone, cooling is small in this region (see the slight decrease in temperature that occurs in point P2, which is located just 10 m away from the injection well). The higher permeability of the fracture zone permits a larger advance of the cooling front, not only in extension, but also in magnitude. Figure 7c displays the spatial distribution of temperature after 2 years of injection, showing that it mainly advances through the fracture zone, but significantly behind the CO_2 front (Figure 7b). Figure 7c also shows a zone of slightly increased temperature that coincides with the CO_2 plume. This small temperature increase, which is lower than 1 ºC, is due to CO_2 dissolution into the brine.

14

Thermal effects on injectivity at In Salah

Figure 8 shows the evolution of the liquid saturation at several points when injecting CO_2 at 50 °C for 30 years using the same material properties as in the calibrated model. Simulation results indicate a rapid desaturation of the whole fracture zone. Actually, CO_2 reaches the limit of the fracture zone (point P5) in half a year. For a continuous CO_2 injection rate of 0.3 Mt/yr, CO_2 breakthrough at point P6, which corresponds to the location of well KB-5, occurs after 1.36 years from the start of injection. In contrast, CO_2 advances much slower in the rest of the reservoir. CO_2 reaches point P4, which is placed 250 m away from the injection well outside the fracture zone, after 3.2 years. CO_2 saturation remains practically constant at every point in the longer-term, until the end of the injection at 30 years.

Figure 9 displays the temperature evolution at the same points as in Figure 8 when injecting CO_2 at 50 °C for 30 years. Cooling takes place rapidly within the fracture zone. Point P1, which is the closest observation point to the injection well, quickly reacts to the cold injection, with a temperature decrease of about 20 ˚C in less than one year. After this rapid temperature drop, the reactivation of the fracture zone enhances its permeability, reducing fluid pressure, which induces an incoming flow of warmer fluid from the surrounding rock that causes a little increase in temperature at about 1 year, only to keep decreasing as the cold injection continues (Figure 8, blue solid line). Point P3, placed 250 m away from the injection well inside the fracture zone, starts to cool down after around 0.3 years and progressively cools down for 20 years, when the injection temperature is almost reached. The cooling front reaches the limit of the fracture zone (point P5), placed 2.5 km away from the injection well, after around 6 years. However, far away from the injection well, the magnitude of the cooling is smaller than around the injection well. On the other hand, outside of the fracture zone, cooling is limited to the vicinity of the injection

 15

well. For example, temperature drops only 5 °C at point P2, which is located 10 m away from the injection well.

This calculated distribution of cooling indicates that, around well KB-502 at In Salah, thermo-mechanical effects may be restricted mainly to the fracture zone and therefore have little effect on the rest of the reservoir. Table 3 quantifies, at point P3, placed 250 m away from the injection well in the fracture zone, the maximum change in the effective stress normal to fractures, which are oriented perpendicular to the well for all the considered cases. This include the base case with the material parameters calibrated against CO_2 injection at well KB-502, an isothermal case, and two cases with a stiffer fracture zone. Additionally, Table 3 includes the ratio of the maximum permeability reached during injection to the initial permeability and the maximum overpressure. The smallest change in the effective stress normal to the fractures occurs in the isothermal case. The smaller the changes in effective stress normal to the fractures, the less the fractures open. Thus, under isothermal conditions, the permeability increase is the smallest and therefore, overpressure is the highest. In contrast, for a cold injection, the changes in effective stress normal to the fractures become larger due to more substantial cooling-induced stresses. As a result, permeability increases more, enhancing injectivity and inducing a lower overpressure. Increasing the stiffness of the fracture zone has the effect of increasing the cooling-induced normal stress reduction, resulting then in a larger permeability ratio and smaller overpressure.

In the cases analyzed here, the injection pressure is high and rapidly reaches the fracturing conditions. Hence, given the small differences in normal stress changes, the effect of cooling-induced stresses is not very large in magnitude because fractures reactivate at the early stage of injection, which causes stress redistribution that limits the effect of the induced cooling stress reduction.

Thermal effects on injectivity at a generic reservoir

16

On the other hand, for the cases in which overpressure is low, i.e., in the homogeneous high permeability models, the effective stress reduction normal to the fractures is initially low and thus, fracture reactivation does not occur due to pressure buildup. However, the effective stress normal to the fractures subsequently decreases due to the induced thermal stresses in the region affected by cooling. As a result, for cooling dominated (instead of pressure dominated) injection scenarios, permeability enhancement due to cooling can be of a factor of three(Figure 10). Note that reactivation, and thus permeability enhancement, only occurs for the case in which CO_2 is injected cold. This permeability enhancement has a clear effect on the required injection pressure to inject a prescribed CO_2 mass flow rate.

Figure 11 displays the overpressure evolution at the injection well and in the reservoir 10 m away from the well for CO_2 injection in thermal equilibrium with the storage formation and at 45 ºC colder than the storage formation. In the reservoir, overpressure is similar despite the higher permeability induced by cooling (Figure 11b). However, the difference becomes significant in the injection well (Figure 11a). Initially, injection pressure builds up slightly more rapidly for the case of cold CO_2 injection due to the higher viscosity of CO_2 for decreasing temperatures. However, after 50 days, the induced thermal stresses are high enough to induce fracture reactivation (Figure 12), which enhances permeability (recall Figure 10). As a result, injection pressure drops more than 1 MPa, which represents around a 20 % of the overpressure. Thus, cold CO_2 injection in cooling dominated injection cases leads to an injectivity enhancement that may give rise to a significant reduction of the injection pressure.

17

DISCUSSION AND CONCLUSIONS

We have calibrated a model of In Salah using the injection data of well KB-502 and the breakthrough time of CO_2 at the well KB-5, obtaining a good fitting. We included a fracture zone perpendicular to the well that caused the double lobe uplift pattern on the ground surface and through which CO_2 rapidly advances, leading to the rapid breakthrough at KB-5. We use a stress-dependent permeability function that predicts an increase in permeability as the effective stress acting normal to the fracture zone decreases. Normal effective stress can decrease either due to overpressure or cooling. Furthermore, we assume that the stress-dependent permeability function can jump to a more permeable function upon reactivation of the fracture zone.

The presence of the fracture zone has a great influence on the CO_2 plume and cooling front evolution (Figure 7). CO_2 preferentially advances through the fracture zone, which becomes two orders of magnitude more permeable than the rest of the reservoir (Figure 6). The slower flow through the reservoir outside of the fracture zone is due to its lower permeability, but more importantly, due to the fact that most of the CO_2 is injected through the fracture zone. Actually, flow rate is not uniformly distributed along wells and will tend to preferentially enter into the storage formation through the zones with the lowest resistance to flow (Rinaldi and Rutqvist, 2013; Vilarrasa et al., 2013b; Chen et al., 2014). This preferential flow also restricts the cooling advance to the fracture zone, which causes a positive feedback for preferential flow as permeability in the fracture zone will be enhanced by cooling. On the other hand, since zones with higher permeability may have a higher fracture density than less permeable zones, the higher fracture density may lead to a softer rock and therefore, induced thermal stresses may become relatively small. However, the temperature difference in CO_2 storage projects may be large (recall the 45 °C difference at In Salah or the 55 °C difference at Cranfield), so even for

18

relatively soft rocks, which may have Young’s modulus in the order of 1 GPa, the induced thermal stresses may still become significant.

To assess the effect of cooling on injectivity, we perform long-term simulations injecting CO_2 at 50 °C at a constant mass flow rate of 0.3 Mt/yr during 30 years. In these simulations, in which we use the calibrated material parameters, pressure buildup is high and approaches the fracturing pressure. We compared cold CO_2 with a case of CO_2 injection in thermal equilibrium with the storage formation, and two extra cases in which we consider a stiffer fracture zone. Simulation results indicate that cooling has the potential to increase injectivity. However, due to the high injection pressure at In Salah, which was close to the fracturing pressure and even exceeded it within the reservoir at some periods of time (Rutqvist, 2012; Oye et al., 2013), fracture reactivation mainly happened due to overpressure. Thus, the effect of cooling was limited in the pressure dominated simulations.

On the other hand, cooling has a larger effect on injectivity when overpressure is low. Since cooling causes a thermal stress reduction, large temperature differences and/or stiff rocks may lead to large effective stress reduction that could yield shear failure conditions. In such cases, permeability would be enhanced, especially in the direction perpendicular to shear, due to the roughness of fractures (Yeo et al., 1998; Mallikamas and Rajaram, 2005; Vilarrasa et al., 2011; Rutqvist, 2015). The increase in injectivity induced by cooling may decrease the injection pressure by 20 % (Figure 11). Data from several injection sites will be required to generalize the actual amount of injectivity increase induced by cooling, but this study suggests that there is potential to save a significant amount of compression energy all over the duration of injection projects. Similar observations of injectivity enhancement have been observed in fractured geothermal reservoirs as a result of strong cooling (e.g., Koh et al., 2011; Jeanne et al., 2015).

19

Overall, our simulation results show that cooling has the potential to enhance injectivity in fractured reservoirs. While in pressure dominated storage sites, like In Salah, most of the permeability enhancement will be due to overpressure, thermal effects will enhance injectivity in cooling dominated storage sites. Cooling dominated injection scenarios are most likely to occur than pressure dominated ones because regulators will, in most cases, limit overpressure below the fracturing pressure to avoid damaging the caprock sealing capacity. Coupled thermo-hydro-mechanical studies should be performed case specifically to assess caprock stability. If the induced thermal stresses do not compromise the caprock integrity and sealing capacity, cooling will be beneficial for CO_2 storage purposes due to the induced permeability and injectivity enhancement.

ACKNOWLEDGMENTS

This work was supported by the Assistant Secretary for Fossil Energy, Office of Natural Gas and Petroleum Technology, through the National Energy Technology Laboratory, under the U.S. Department of Energy Contract No. DE-AC02-05CH11231. V. Vilarrasa acknowledges financial support from the “TRUST" project (European Community's Seventh Framework Programme FP7/2007-2013 under grant agreement n. 309607) and from “FracRisk" project (European Community's Horizon 2020 Framework Programme H2020-EU.3.3.2.3 under grant agreement n. 640979). A.P. Rinaldi is currently funded by Swiss National Science Foundation (SNSF) Ambizione Energy grant (PZENP2_160555). The authors would like to thank the In Salah JIP and their partners BP, Statoil, and Sonatrach for providing field data and technical input over the past 10 years as well as for financial support during LBNL's participation in the In Salah JIP, 2011–2013.

 20

REFERENCES

Bao, J., Xu, Z., Fang, Y., 2014. A coupled thermal-hydro-mechanical simulation for carbon dioxide sequestration. *Environmental Geotechnics* doi:10.1680/envgeo.14.00002.

Bear, J. (ed.), 1972. *Dynamics of fluids in porous media*. Elsevier, New York.

Bissell, R.C., Vasco, D.W., Atbi, M., Hamdani, M., Okwelegbe, M., Goldwater, M.H., 2011. A full field simulation of the In Salah gas production and CO_2 storage project using a coupled geo-mechanical and thermal fluid flow simulator. *Energy Procedia* 4:3290–3297.

Birkholzer, J.T., Oldenburg, C.M., Zhou, Q., 2015. CO_2 migration and pressure evolution in deep saline aquifers. *International Journal of Greenhouse Gas Control* 40:203-220.

Chen, F., Wiese, B., Zhou, Q., Kowalsky, M. B., Norden, B., Kempka, T., Birkholzer, J. T., 2014. Numerical modeling of the pumping tests at the Ketzin pilot site for CO_2 injection: model calibration and heterogeneity effects. *International Journal of Greenhouse Gas Control*, 22:200-212.

De Simone, S., Vilarrasa, V., Carrera, J., Alcolea, A., Meier, P., 2013. Thermal coupling may control mechanical stability of geothermal reservoirs during cold water injection. *Journal of Physics and Chemistry of the Earth* 64:117-126.

Fang, Y., Nguyen, B.N., Carroll, K., Xu, Z., Yabusaki, S.B., Scheibe, T.D., Bonneville, A., 2013. Development of a coupled thermo-hydro-mechanical model in discontinuous media for carbon sequestration. *International Journal of Rock Mechanics and Mining Sciences* 62:138–147.

Finsterle, S., 2007. *iTOUGH2 User's Guide*, Report LBNL-40040, Lawrence Berkeley Natl. Lab., Berkeley, CA, USA.

Finsterle, S., and Zhang, Y., 2011. Solving iTOUGH2 simulation and optimization using PEST protocol, *Environ. Modell. Softw.*, 26(7), 959-968.

 21

Gemmer, L., Hansen, O., Iding, M., Leary, S., Ringrose, P., 2012. Geomechanical response to CO_2 injection at Krechba, In Salah, Algeria. *First Break* 30(2):79-84.

Goodarzi, S., Settari, A., Keith, D., 2012. Geomechanical modeling for CO_2 storage in Nisku aquifer in Wabamun lake area in Canada. *International Journal of Greenhouse Gas Control* 10:113–122.

Goodarzi, S., Settari, A., Zoback, M.D., Keith, D.W., 2015. Optimization of a CO_2 storage project based on thermal, geomechanical and induced fracturing effects. *Journal of Petroleum Science and Engineering* 134:49-59.

Gor, Y.G., Elliot, T.R., Prévost, J.H., 2013. Effects of thermal stresses on caprock integrity during CO_2 storage. *International Journal of Greenhouse Gas Control* 12:300–309.

Han, W.S., Stillman, G.A., Lu, M., Lu, C., McPherson, B.J., Park, E., 2010. Evaluation of potential non isothermal processes and heat transport during CO_2 sequestration. *Journal of Geophysical Research* 115, B07209, doi: 10.1029/2009JB006745.

Iding, M., Ringrose, P., 2010. Evaluating the impact of fractures on the performance of the In Salah CO_2 storage site. *International Journal of Greenhouse Gas Control* 4:242-248.

IEAGHG, 2013. Induced seismicity and its implications for CO_2 storage risk. 2013/09, June 2013.

ITASCA, 2009. *FLAC3d v5.0, Fast Lagrangian Analysis of Continua in 3 Dimensions, User's Guide*. Minneapolis, MN, USA: Itasca Consulting Group.

Jeanne, P., Rutqvist, J., Rinaldi, A. P., Dobson, P. F., Walters, M., Hartline, C., Garcia, J., 2015. Seismic and aseismic deformations and impact on reservoir permeability: The case of EGS stimulation at The Geysers, California, USA. *Journal of Geophysical Research: Solid Earth*, 120(11):7863-7882.

 22

Kim, S., Hosseini, S. A., 2014. Above-zone pressure monitoring and geomechanical analyses for a field-scale CO_2 injection project in Cranfield, MS. *Greenhouse Gases: Science and Technology* 4(1):81-98.

Kim, S., Hosseini, S.A., 2015. Hydro-thermo-mechanical analysis during injection of cold fluid into a geologic formation. *International Journal of Rock Mechanics and Mining Sciences*, 77:220-236.Koh, J., Roshan, H., Rahman, S. S., 2011. A numerical study on the long term thermo-poroelastic effects of cold water injection into naturally fractured geothermal reservoirs. *Computers and Geotechnics*, 38(5):669-682.

Liu, H. H., Rutqvist, J., Berryman, J. G., 2009. On the relationship between stress and elastic strain for porous and fractured rock. *International Journal of Rock Mechanics and Mining Sciences*, 46(2):289-296.

Liu, H.H., Wei, M.Y., Rutqvist, J., 2013. Normal-stress dependence of fracture hydraulic properties including two-phase flow properties. *Hydrogeology Journal* 21(2):371-382.

Liu, H.H., and Rutqvist, J., 2013. Coupled hydromechanical processes associated with multiphase flow in a dual-continuum system: formulations and an application, *Rock Mech. Rock Eng.*, 46(5), 1103-1112.

Mallikamas, W., Rajaram, H., 2005. On the anisotropy of the aperture correlation and effective transmissivity in fractures generated by sliding between identical self-affine surfaces. *Geophysical Research Letters*, 32 L11401.

Mathieson, A., Wright, I., Roberts, D., Ringrose, P., 2009. Satellite imaging to monitor CO_2 movement at Krechba, Algeria. *Energy Procedia* 1(1):2201-2209.

Morris, J.P., Hao, Y., Foxall, W., McNab, W., 2011. A study of injection-induced mechanical deformation at the In Salah CO_2 storage project. *International Journal of Greenhouse Gas Control* 5(2):270-280.

 23

Nield, D.A., Bejan, A., 2006.*Convection in porous media*. Springer, New York.

Onuma, T., Ohkawa, S., 2009. Detection of surface deformation related with CO_2 injection by DInSAR at In Salah, Algeria. *Energy Procedia* 1(1):2177-2184.

Oye, V., Aker, E., Daley, TM., Kühn, D., Bohloli, B., Korneev, V. 2013. Microseismic monitoring and interpretation of injection data from the In Salah CO_2 storage site (Krechba), Algeria. *Energy Procedia* 37:4191–4198.

Pan, L., Oldenburg, C. M., Pruess, K., and Wu, Y.-S., 2011. Transient CO_2 leakage and injection in wellbore-reservoir system for geological carbon sequestration, *Greenh. Gas. Sci. Tech.*, 1(4), 335-350.

Paterson, L., Lu, M., Connell, L.D., Ennis-King, J., 2008. Numerical modeling of pressure and temperature profiles including phase transitions in carbon dioxide wells. *SPE Annual Technical Conference and Exhibition*, Denver, 21-24 September 2008.

Preisig, M., Prévost, J.H., 2011. Coupled multi-phasse thermo-poromechanical effects. Case study: CO_2 injection at In Salah, Algeria. *International Journal of Greenhouse Gas Control* 5(4):1055–1064.

Pruess, K., 2005. *ECO2N: A TOUGH2 Fluid Property Module for Mixtures of Water, NaCl, and CO_2*. Paper LBNL- 57952. Lawrence Berkeley Natl. Lab., Berkeley, CA, USA.

Pruess, K., Oldenburg, C. M., Moridis, G., 2011. *TOUGH2 User's Guide, Version 2.1*. Lawrence Berkeley Natl. Lab., Berkeley, CA, USA: Paper LBNL-43134 (revised).

Rinaldi, A.P., Rutqvist, J., 2013. Modeling of deep fracture zone opening and transient ground surface uplift at KB-502 CO_2 injection well, In Salah, Algeria. *International Journal of Greenhouse Gas Control* 12:155–167.

 24

Rinaldi, A.P., Rutqvist, J., Finsterle, S., Liu, H.H., 2014a. Forward and inverse modeling of ground surface uplift at In Salah, Algeria. In *48th US Rock Mechanics/Geomechanics Symposium*. American Rock Mechanics Association.

Rinaldi, A.P., Jeanne, P., Rutqvist, J., Cappa, F., Guglielmi, Y., 2014b. Effects of fault-zone architecture on earthquake magnitude and gas leakage related to CO_2 injection in a multi-layered sedimentary system. *Greenhouse Gas: Science and Technology* 4:99-120, doi:10.1002/ghg.1403.

Rinaldi, A.P., Rutqvist, J., Finsterle, S., and Liu, H.H., 2015a. Inverse modeling of coupled fluid flow and geomechanics with iTOUGH2-PEST and TOUGH-FLAC: Application to In Salah CO_2 storage site, *TOUGH Symposium 2015*, Berkeley, CA, USA, 28-30 September, 2015.

Rinaldi, A. P., Vilarrasa, V., Rutqvist, J., Cappa, F., 2015b. Fault reactivation during CO_2 sequestration: Effects of well orientation on seismicity and leakage. *Greenhouse Gases: Science and Technology*5(5): 645-656.

Rinaldi, A. P., Rutqvist, J., Finsterle, S., Liu, H. H., 2016. Inverse modeling of ground surface uplift and pressure with iTOUGH-PEST and TOUGH-FLAC: The case of CO_2 injection at In Salah, Algeria. *Computers & Geosciences*, doi: 10.1016/j.cageo.2016.10.009.

Ringrose, P., Atbi, M., Mason, D., Espinassous, M., Myhrer, Ø., Iding, M., Mathieson, A., Wright, I., 2009. Plume development around well KB-502 at the In Salah CO_2 storage site. *First break* 27(1):85-89.

Rucci, A., Vasco, D. W., Novali., F., 2013. Monitoring the geological storage of carbon dioxide using multicomponent SAR interferometry. *Geophys. J. Int.* 193(1): 197-208.

Rutqvist, J., Wu, Y.S., Tsang, C.F., Bodvarsson, G.S., 2002. A modeling approach for analysis of coupled multiphase fluid flow, heat transfer, and deformation in fractured porous rock. *International Journal of Rock Mechanics and Mining Sciences*39:429–42.

25

Rutqvist, J., Vasco, D.W., Myer, L., 2010. Coupled reservoir-geomechanical analysis of CO_2 injection and ground deformations at In Salah, Algeria. *International Journal of Greenhouse Gas Control* 4(2):225–230.

Rutqvist, J., 2011. Status of TOUGH-FLAC simulator and recent applications related to coupled fluid flow and crustal deformations. *Comput. Geosci.* 37:739-750.

Rutqvist, J., Liu, H.H., Vasco, D.W., Pan, L., Kappler, K., Majer, E., 2011. Coupled non-isothermal, multiphase fluid flow, and geomechanical modeling of ground surface deformations and potential for induced micro-seismicity at the In Salah CO_2 storage operation. *Energy Procedia* 4:3542-3549.

Rutqvist, J., 2012. The geomechanics of CO_2 storage in deep sedimentary formations. *International Journal of Geotechnical and Geological Engineering* 30:525–551.

Rutqvist, J., 2015. Fractured rock stress-permeability relationships from in situ data and effects of temperature and chemical-mechanical couplings. *Geofluids* 15(1-2): 48-66.

Rutqvist, J., Rinaldi, A.P., Cappa, F., Jeanne, P., Mazzoldi, A., Urpi, L., Guglielmi, Y. and Vilarrasa, V., 2016. Fault activation and induced seismicity in geologic carbon storage - Lessons learned from recent modeling studies.*Journal of Rock Mechanics and Geotechnical Engineering* 8: 789-804.

Segall, P., Fitzgerald, S.D., 1998. A note on induced stress changes in hydrocarbon and geothermal reservoirs. *Tectonophysics* 289:117-128.

Shi, J.-Q., Sinayuc, C., Durucan, S., Korre, A., 2012. Assessment of carbon dioxide plume behavior within the storage reservoir and the lower caprock around the KB-502 injection well at In Salah. *International Journal of Greenhouse Gas Control* 7:115-126.

 26

Singh, A.K., Goerke, U.-J., Kolditz, O., 2011. Numerical simulation of non-isothermal compositional gas flow: Application to carbon dioxide injection into gas reservoirs. *Energy* 36:3446-3458.

Spycher, N., Pruess, K., 2005. CO_2-H_2O mixtures in the geological sequestration of CO_2. II. Partitioning in chloride brines at 12–100 C and up to 600 bar. *Geochimica et Cosmochimica Acta*, 69(13):3309-3320.

Stork, A.L., Verdon, J.P., Kendall, J.M., 2015. The microseismic response at the In Salah Carbon Capture and Storage (CCS) site. *International Journal of Greenhouse Gas Control*32: 159-171.

Vasco, D.W., Ferretti, A., Novali, F., 2008. Reservoir monitoring and characterization using satellite geodetic data: interferometric synthetic aperture radar observations from the Krechba field, Algeria. *Geophysics* 73(6), WA113–WA122.

Vasco, D.W., Rucci, A., Ferretti, A., Novali, F., Bissell, R.C., Ringrose, P.S., Mathieson, A., Wright, I.W., 2010. Satellite-based measurements of surface deformation reveal fluid flow associated with the geological storage of carbon dioxide. *Geophysical Research Letters* 37(3), L03303, doi:10.1029/2009GL041544.

Verdon, J.P., Kendall, J.M., Stork, A.L., Chadwick, R.A., White, D.J. and Bissell, R.C., 2013. Comparison of geomechanical deformation induced by megatonne-scale CO_2 storage at Sleipner, Weyburn, and In Salah. *Proceedings of the National Academy of Sciences* 110(30):E2762-E2771.

Verdon, J.P., Stork, A.L., Bissell, R.C., Bond, C.E., Werner, M.J., 2015. Simulation of seismic events induced by CO_2 injection at In Salah, Algeria. *Earth and Planetary Science Letters* 426: 118-129.

 27

Vilarrasa, V., Koyama, T., Neretnieks, I., Jing, L., 2011. Shear-induced flow channels in a single rock fracture and their effect on solute transport. *Transport in Porous Media*, 87(2): 503-523.

Vilarrasa, V., Silva, O., Carrera, J., Olivella, S., 2013a. Liquid CO_2 injection for geological storage in deep saline aquifers. *International Journal of Greenhouse Gas Control* 14:84–96.

Vilarrasa, V., Carrera, J., Bolster, D., Dentz, M., 2013b. Semianalytical solution for CO_2 plume shape and pressure evolution during CO_2injection in deep saline formations. *Transport in Porous Media* 97(1): 43-65.

Vilarrasa, V., Olivella, S., Carrera, J., Rutqvist, J., 2014. Long term impacts of cold CO_2 injection on the caprock integrity. *International Journal of Greenhouse Gas Control* 24:1-13.

Vilarrasa, V., Rutqvist, J., Rinaldi, A.P., 2015. Thermal and capillary effects on the caprock mechanical stability at In Salah, Algeria. *Greenhouse Gases: Science and Technology* 5(4): 449-461.

Vilarrasa, V., 2016. The role of the stress regime on microseismicity induced by overpressure and cooling in geologic carbon storage. *Geofluids*, doi: 10.1111/gfl.12197.

Vilarrasa, V., Rutqvist, J., 2017. Thermal effects on geologic carbon storage. *Earth Science Reviews*, 165:245-256

White, J.A., Chiaramonte, L., Ezzedine, S., Foxall, W., Hao, Y., Ramirez, A., McNab, W., 2014. Geomechanical behavior of the reservoir and caprock system at the In Salah CO_2 storage project. *Proceedings of the National Academy of Sciences* doi:10.1073/pnas.1316465111.

Witherspoon, P.A., Wang, J.S.Y., Iwai, K., Gale, J.E., 1980. Validity of cubic law for fluid flow in a deformable rock fracture. *Water Resources Research* 16:1016–1024.

 28

Yeo, I. W., De Freitas, M. H., Zimmerman, R. W., 1998. Effect of shear displacement on the aperture and permeability of a rock fracture. *International Journal of Rock Mechanics and Mining Sciences*, 35(8):1051-1070.

29

TABLES

Table 1. Properties of the rocks considered in the fracture model of In Salah, Algeria.

Property	Fracture	Rock matrix
Intrinsic permeability, k (m^2)	10^{-12}	$1.3 \cdot 10^{-14}$
Relative water permeability, k_{rw} (-)	S_w^3	$S_w^{5.25}$
Relative CO_2 permeability, k_{rc} (-)	S_c^3	$S_c^{3.5}$
Gas entry pressure, p_0 (MPa)	0.01	0.1
van Genuchten shape parameter m (-)	0.8	0.7
Residual liquid saturation, S_{rw} (-)	0.05	0.31
Porosity (-)	0.5	0.17
Thermal conductivity of geologic media, λ (W/m/K)	2.0	2.0
Solid specific heat capacity, c_p (J/kg/K)	900	900
Bulk thermal expansion coefficient, α_T (ºC^{-1})	10^{-5}	10^{-5}

30

Table 2. Properties of the calibrated reservoir model of In Salah, Algeria. The first and second values of volume fractions correspond to before and after reactivation, respectively (note that $\gamma_e + \gamma_t = 1$.

Property	Rock	Fracture zone
Initial intrinsic permeability, k (m^2)	$10^{-14.09\pm0.13}$ ($8.1\cdot10^{-15}$)	$10^{-13.0\pm0.2}$ ($9.5\cdot10^{-14}$)
Bulk modulus reservoir fractures, $K_{t,f}$ (MPa)	3.5±1.2	3.1±1.4
Hard unstressed volume fraction, γ_e (-)	0.2647 – 0.2	0.2647 – 0.001
Soft unstressed volume fraction, γ_t (-)	0.7353 – 0.8	0.7353 – 0.999
Friction angle, φ (-)	26.6 ±1.2	28±1.3
Young's modulus, E (GPa)	10	1
Poisson ratio, ν (-)	0.3	0.3

31

Table 3. Maximum change in the effective stress normal to the fractures at In Salah, $\Delta\sigma_n'$, ratio of the maximum permeability to the initial permeability, $\kappa_{\max}/\kappa_i$, and the maximum overpressure, ΔP, reached during injection at points P3 (250 m away from the injection well inside the fracture zone), for all the considered cases.

Case	$\Delta\sigma_n'$ (MPa)	$\kappa_{\max}/\kappa_i$ (–)	ΔP (MPa)
Base case	-6.50	582	11.46
Isothermal	-6.41	533	11.53
Stiffer fracture zone (factor 5)	-6.74	735	11.42
Stiffer fracture zone (factor 10)	-6.80	783	11.41

32

FIGURES

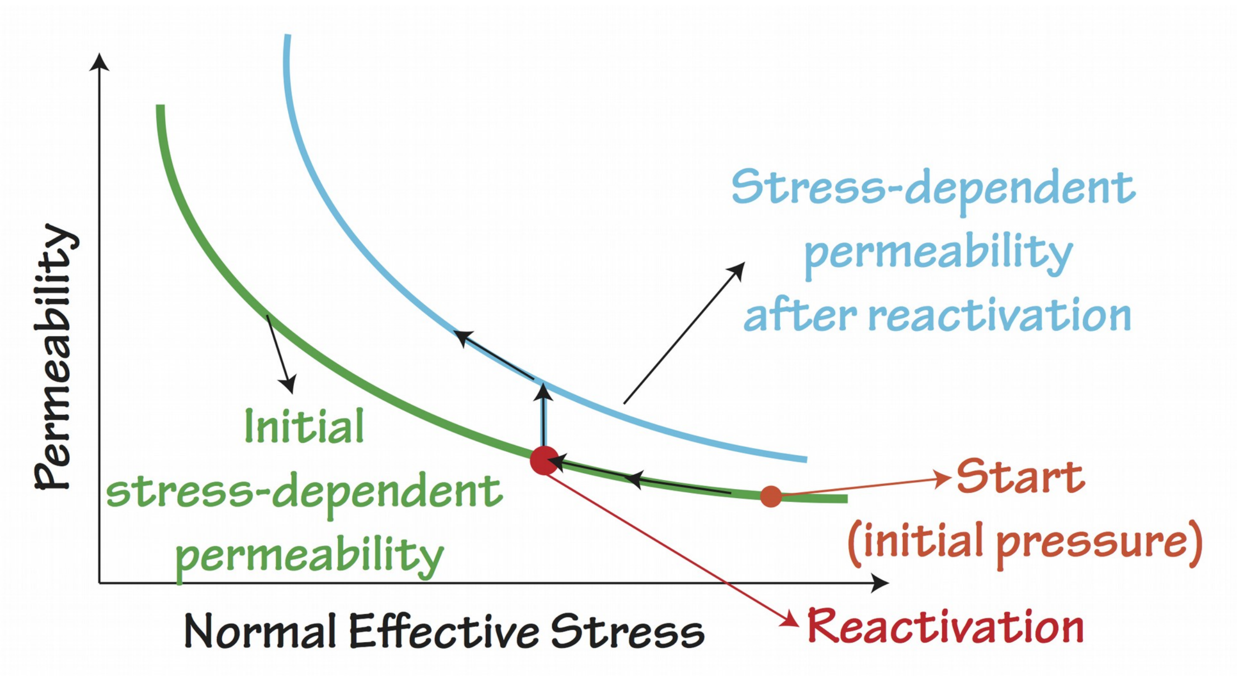

Figure 1. Stress-dependent permeability functions, including permeability changes upon fracture reactivation.

33

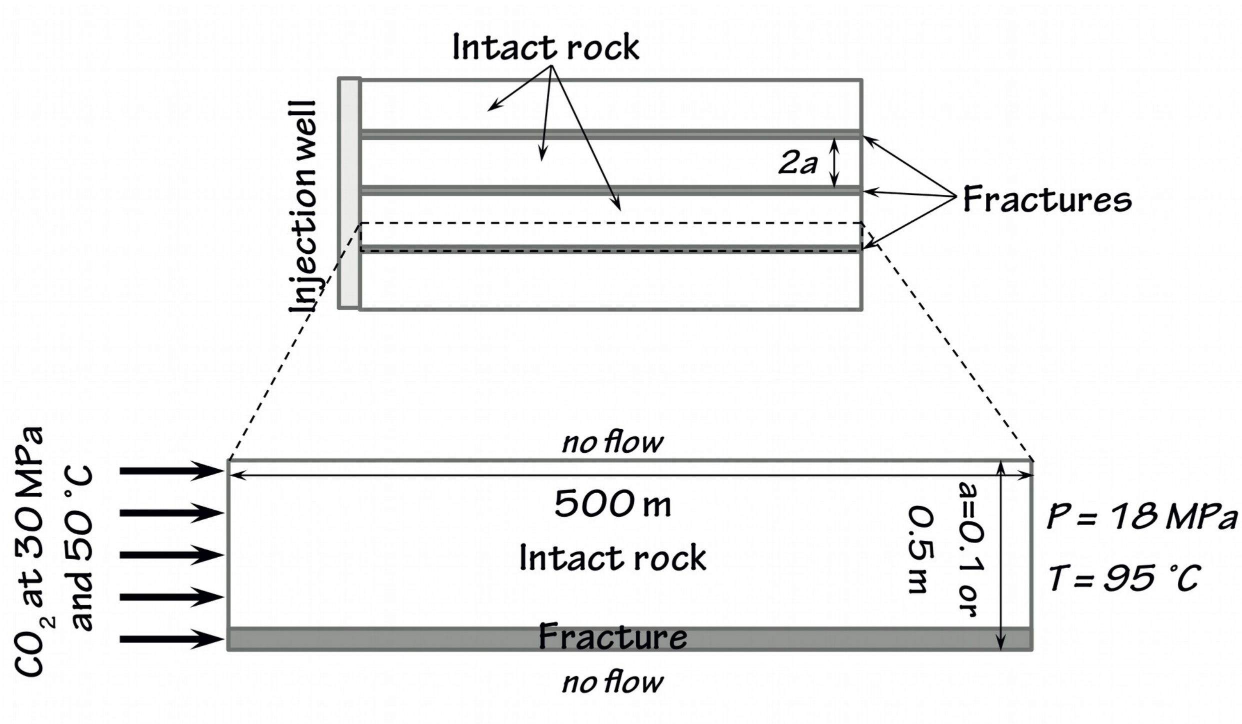

Figure 2. Schematic representation of the model including half of a single fracture and the rock matrix between two adjacent fractures. Note that the fracture has been enlarged in order to visualize it.

34

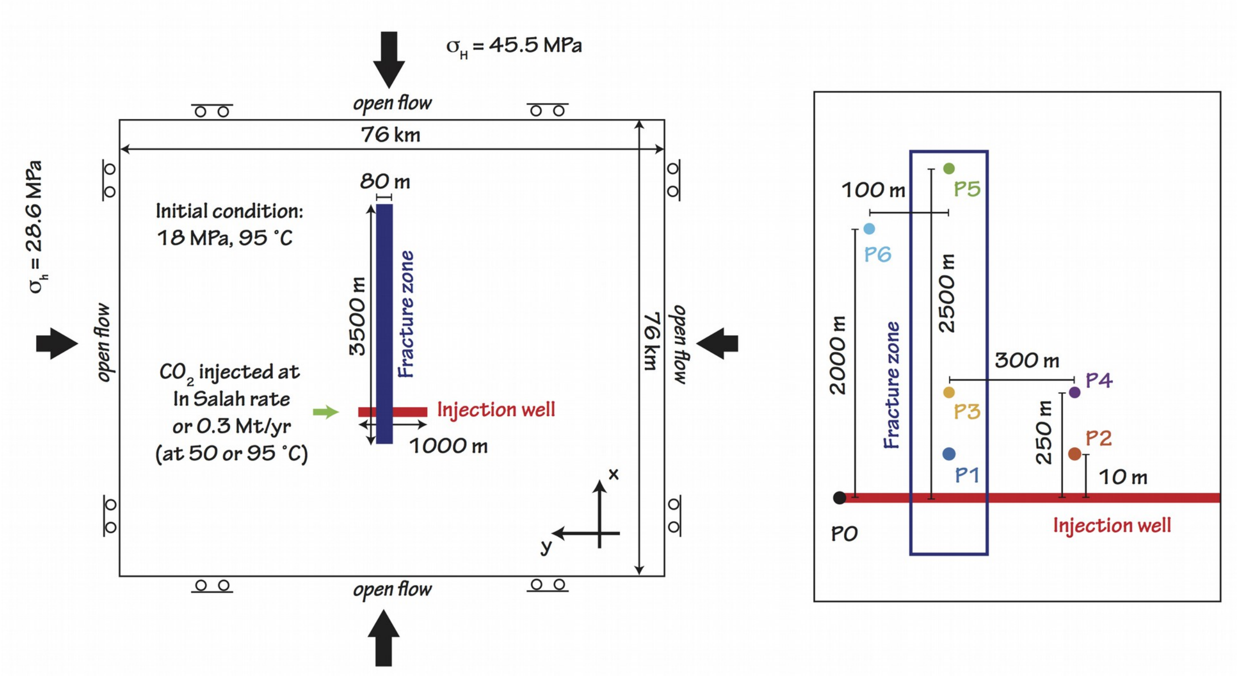

Figure 3. (a) Schematic representation of the model setup, including initial and boundary conditions of the reservoir model around the KB-502 injection horizontal well (red line) at In Salah and (b) position of the monitoring points used in the model. P6 corresponds to the approximate position of vertical well KB-5.

35

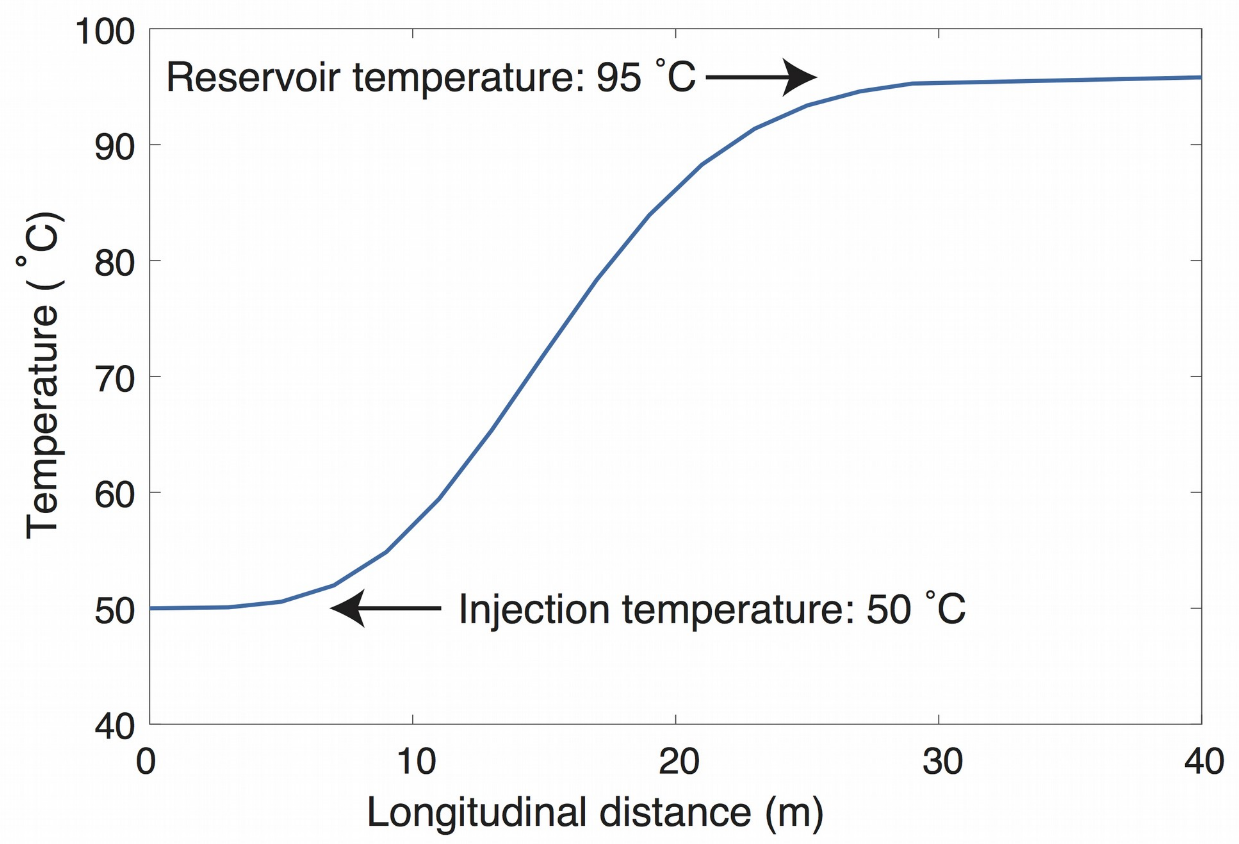

Figure 4. Temperature distribution after 3 days of injection in the model considering a single fracture and the rock matrix around the fracture. The temperature front has a negligible difference between the fracture and the rock matrix, so the modeling of the In Salah reservoir, which is fractured, as an equivalent porous media is valid.

36

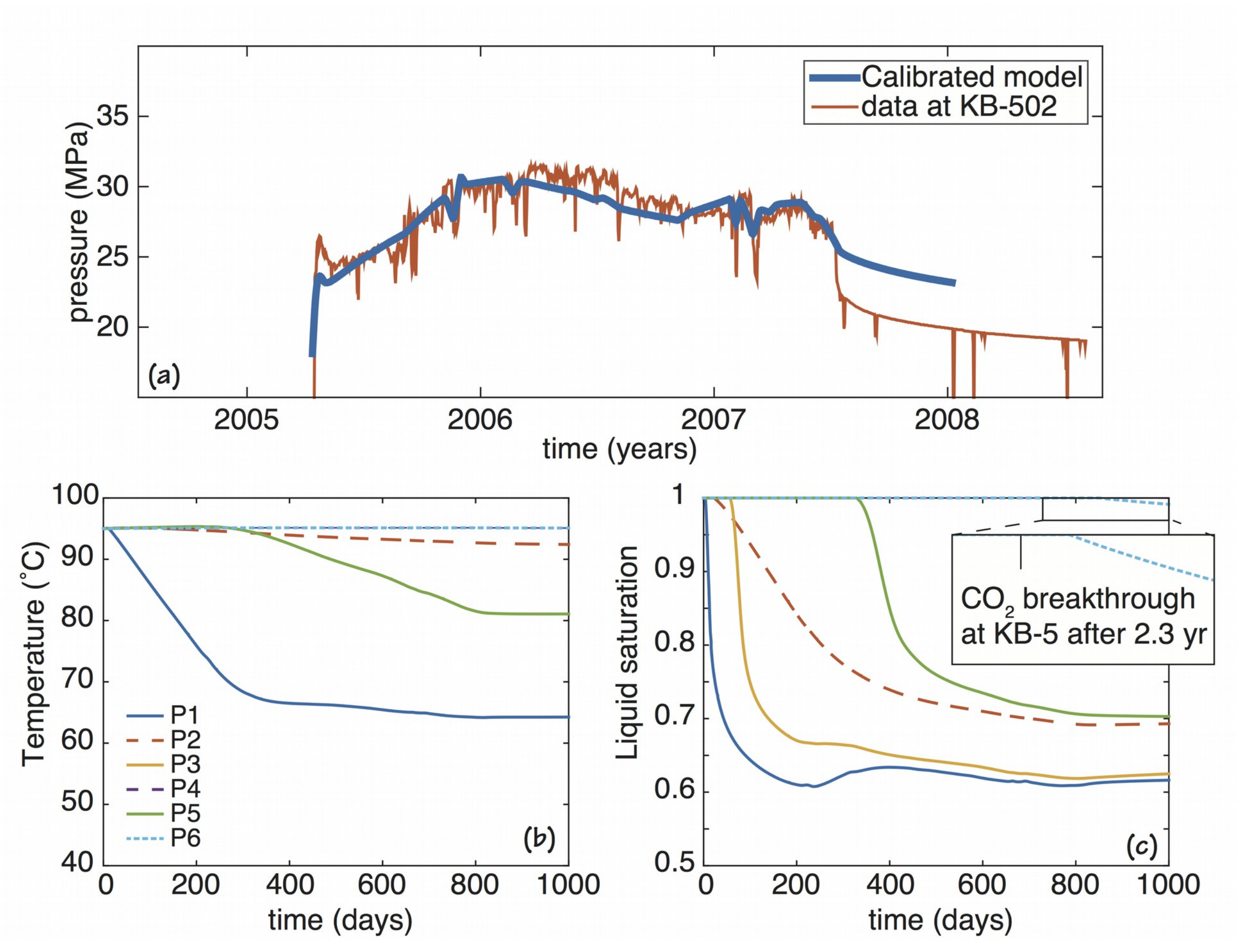

Figure 5. (a) Resulting pressure for the calibrated model compared to measured bottomhole pressure at KB-502 injection well. (b) Temperature and (c) liquid saturation at the six monitoring points as a function of time. While solid lines represent monitoring points within the fracture zone, dashed lines correspond to monitoring points in the reservoir (Figure 3). The cyan dotted line is the KB-5 monitoring point.

37

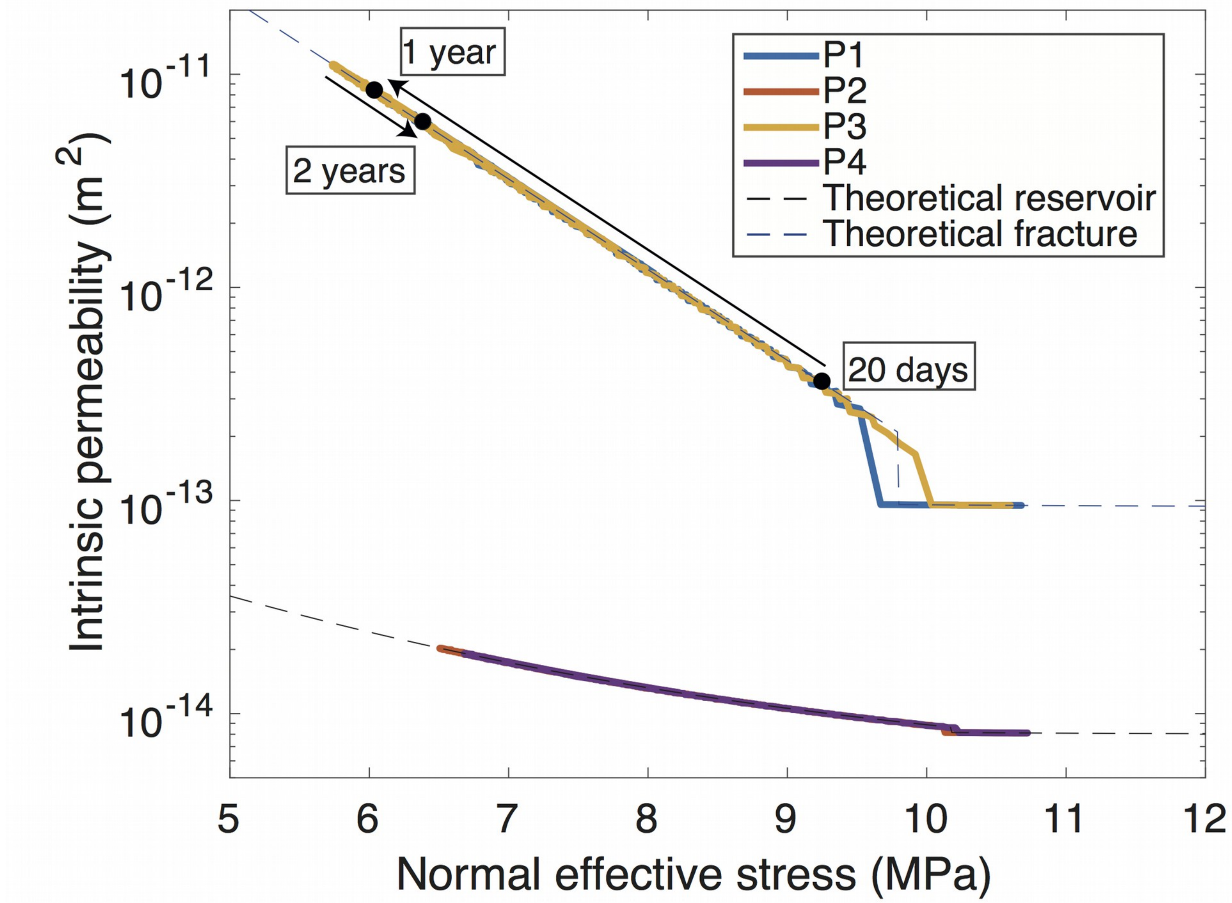

Figure 6. Stress-dependent permeability functions of the fracture zone and the rest of the reservoir, including the permeability enhancement upon fracture reactivation. The permeability evolution with time of points P1 to P3 is also indicated as the effective stress normal to fractures decreases due to overpressure and cooling.

38

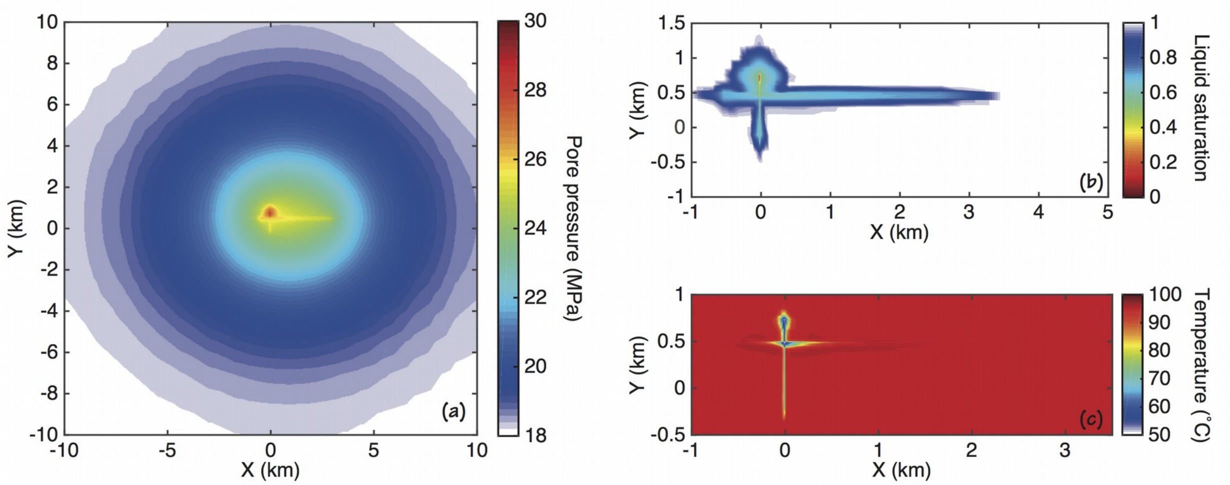

Figure 7. (a) Pressure, (b) liquid saturation and (c) temperature distribution after 2 years of cold CO_2 injection.

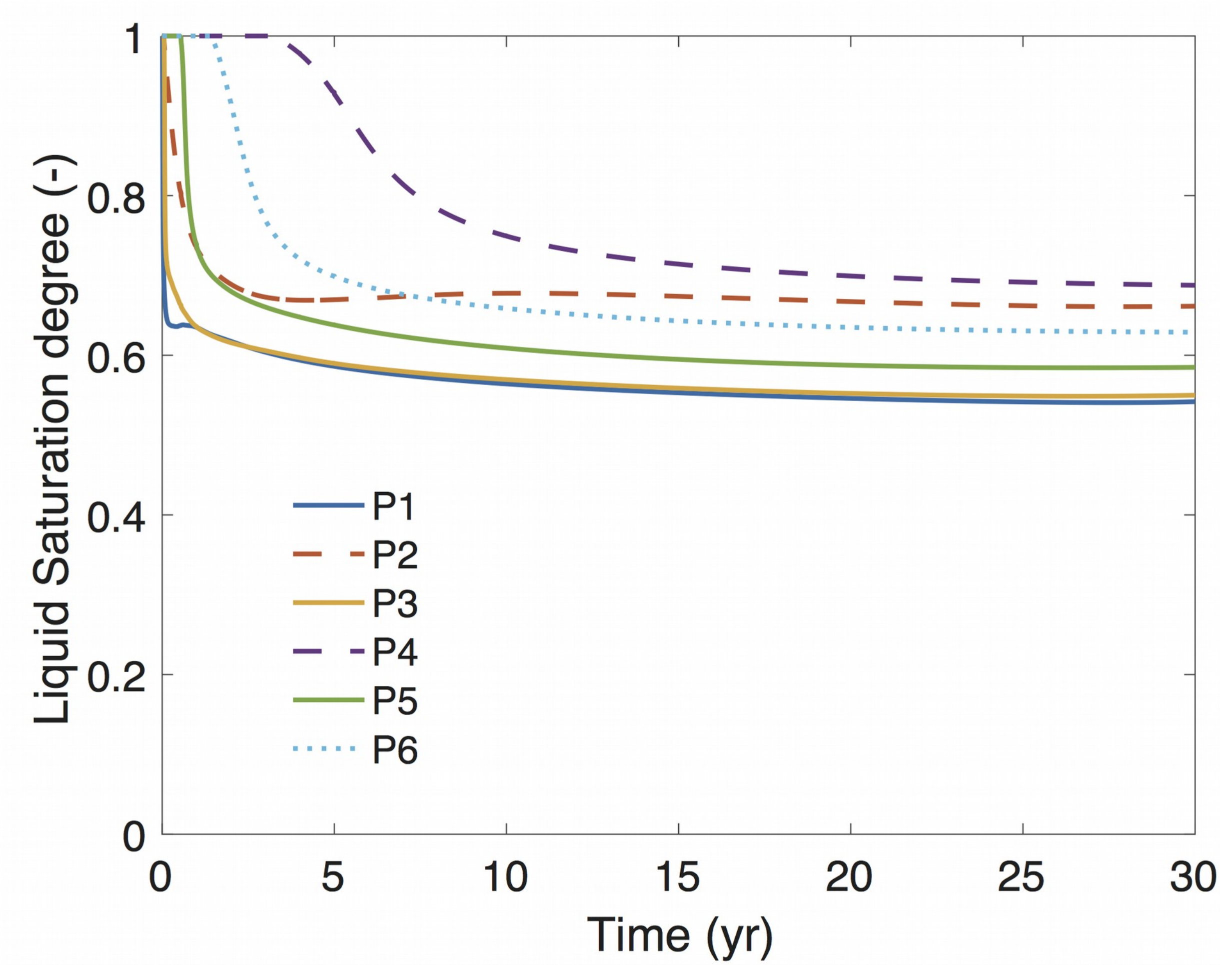

39

Figure 8. Liquid saturation evolution for CO_2 injectionat 50 °C during 30 years at several observation points. While solid lines represent monitoring points within the fracture zone, dashed lines correspond to monitoring points in the reservoir (Figure 3). The cyan dotted line is the KB-5 monitoring point.

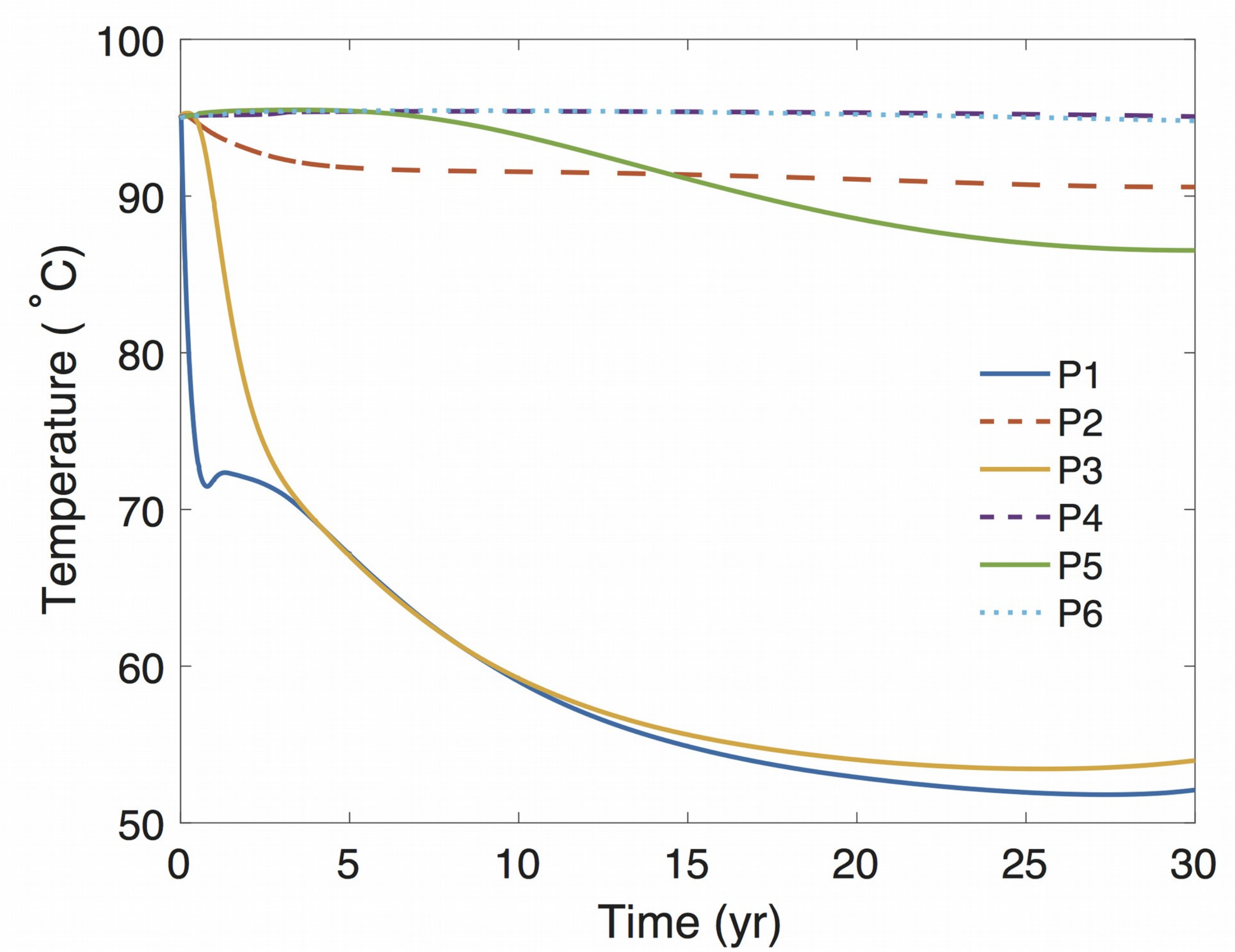

Figure 9. Temperature evolution at several observation points when injecting CO_2 at 50 °C during 30 years. While solid lines represent monitoring points within the fracture zone, dashed lines correspond to monitoring points in the reservoir (Figure 3). The cyan dotted line is the KB-5 monitoring point.

40

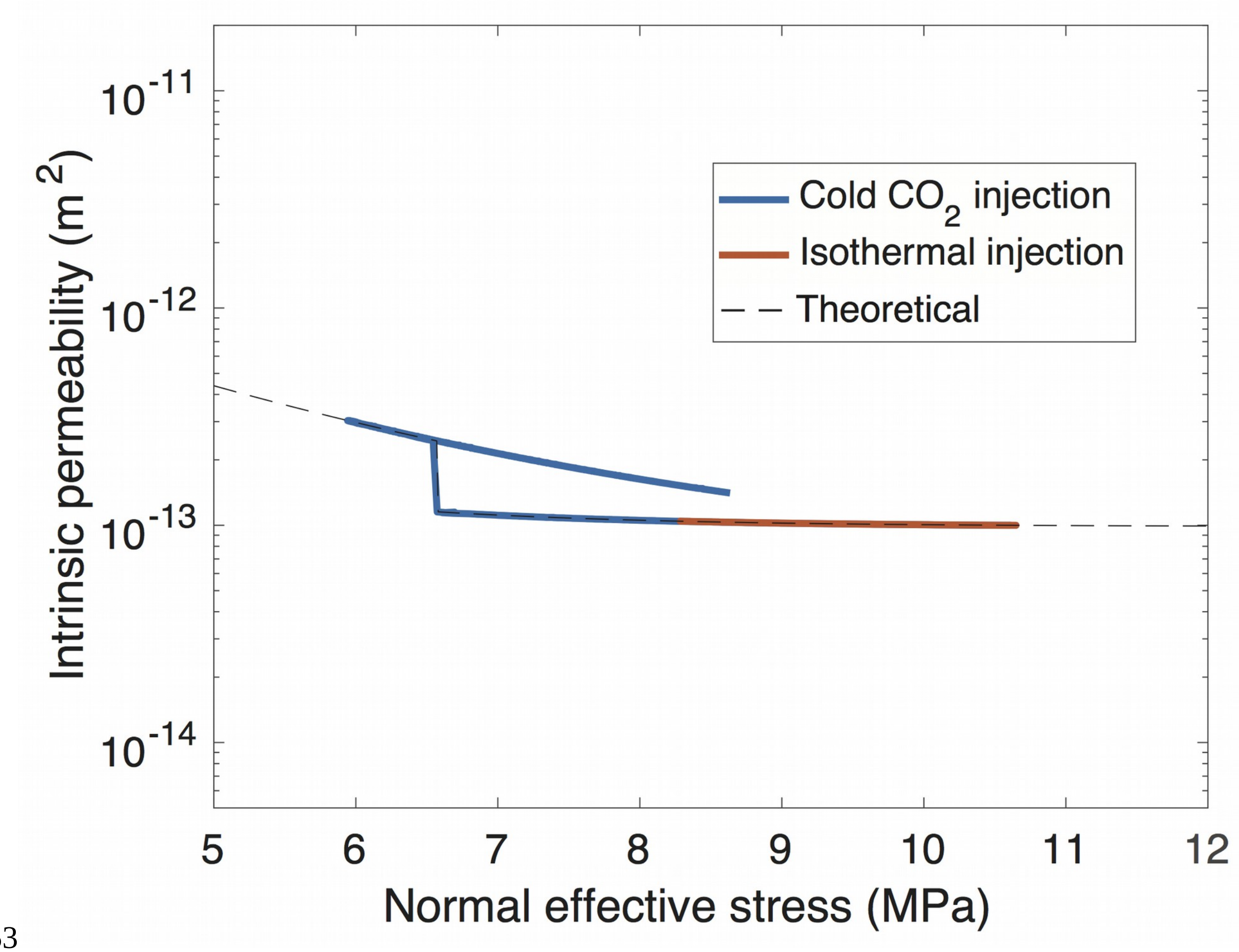

Figure 10. Stress-dependent permeability functions of the high permeable homogeneous models when injecting CO_2 at 50 °C and at 95 ºC during 30 years at observation point P1.

41

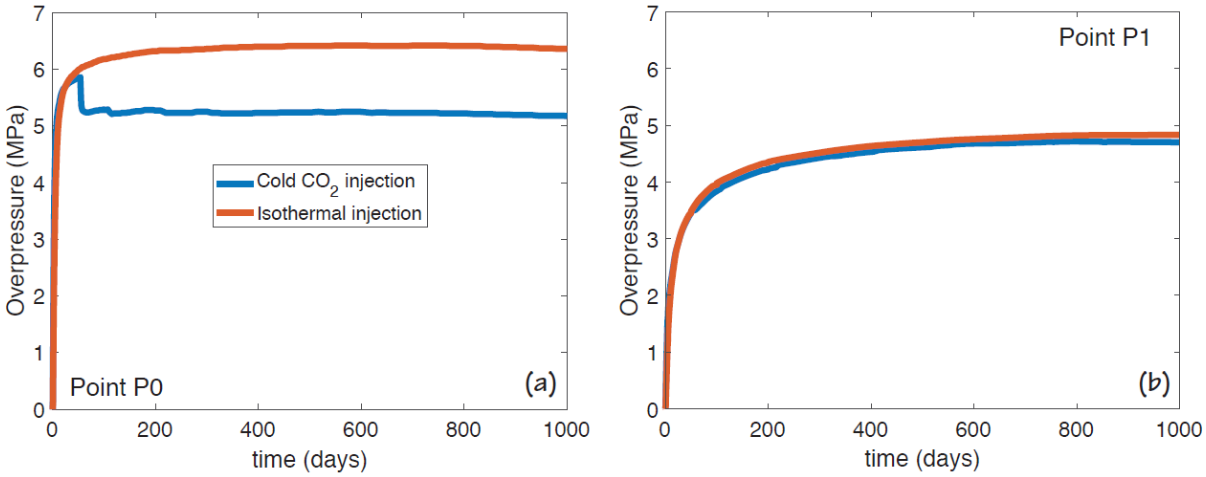

Figure 11. Overpressure evolution (a) at the injection well at point P0 and (b) at point P1for CO_2 injection 45 ºC colder than the storage formation (blue line) and in thermal equilibrium with the storage formation (red line) in a high permeable homogeneous reservoir. The sharp drop in overpressure when injecting cold CO_2 is due to permeability and injectivity enhancement induced by thermal stress reduction.

42

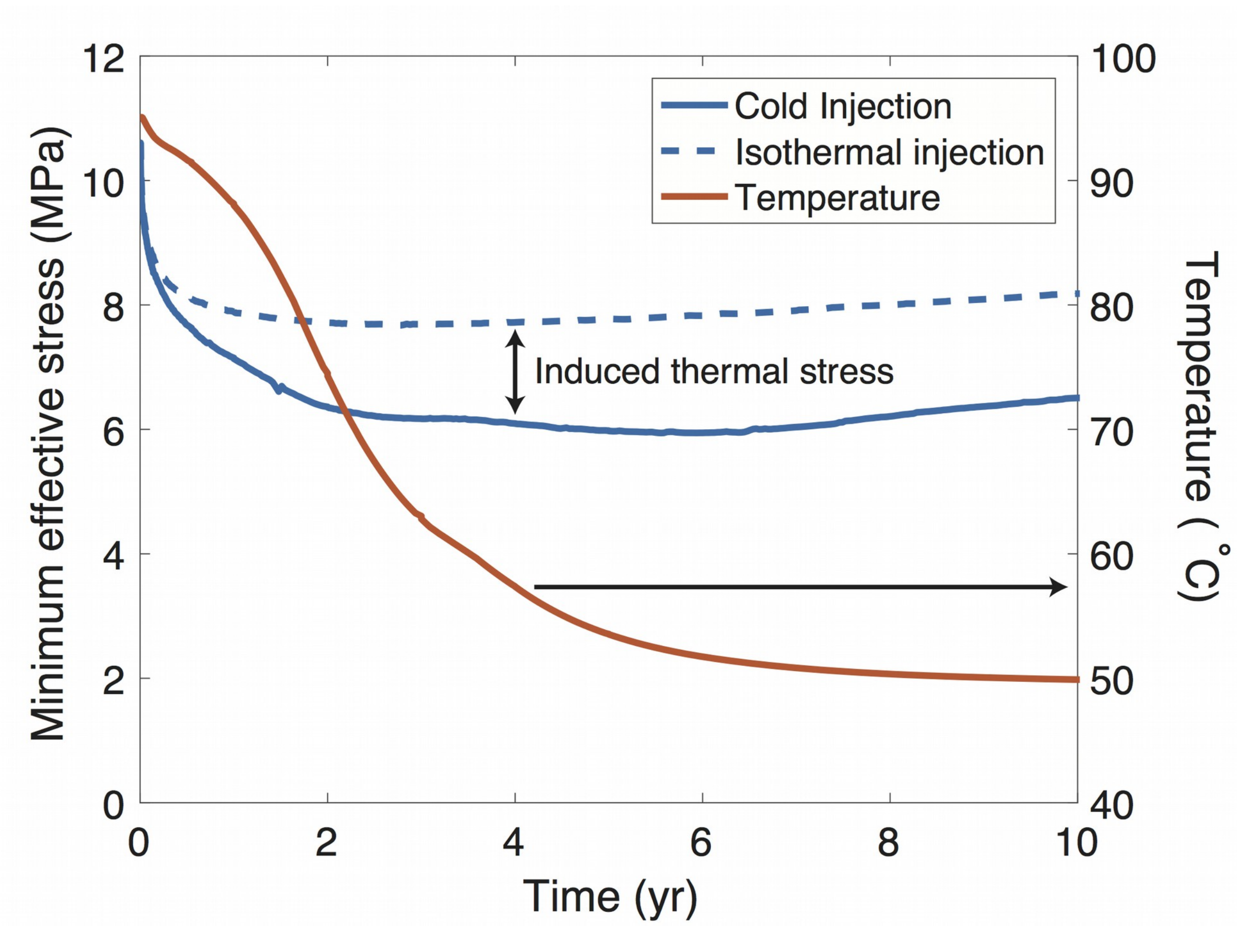

Figure 12. Minimum effective stress evolution at point P1 for CO_2 injection 45 ºC colder than the storage formation and in thermal equilibrium with the storage formation in a high permeable homogeneous reservoir. The difference between the two effective stresses is the induced thermal stress, which is proportional to the temperature reduction indicated for the case of the cold CO_2 injection.

43